EBioMedicine 17 (2017) 145–156

Contents lists available at ScienceDirect

EBioMedicine

journal homepage: www.ebiomedicine.com

Research Paper

A cDNA Clone-Launched Platform for High-Yield Production of Inactivated Zika Vaccine

Yujiao Yang [a,b,1], Chao Shan [a,1], Jing Zou [a], Antonio E. Muruato [c,d], Diniz Nunes Bruno [a,e], Barbosa de Almeida Medeiros Daniele [a,e], Pedro F.C. Vasconcelos [e,j], Shannan L. Rossi [c,f], Scott C. Weaver [c,d,g,h,i], Xuping Xie [a,*], Pei-Yong Shi [a,d,i,j,k,**]

[a] Department of Biochemistry & Molecular Biology, University of Texas Medical Branch, Galveston, TX, USA
[b] College of Animal Science and Technology, Southwest University, Chongqing, China
[c] Institute for Human Infections & Immunity, Galveston, TX, USA
[d] Institute for Translational Science, Galveston, TX, USA
[e] Seção de Arbovirologia e Febres Hemorrágicas, Instituto Evandro Chagas, Ministério da Saúde, Ananindeua, Pará, Brazil
[f] Department of Pathology, Center for Biodefense & Emerging Infectious Diseases, Galveston, TX, USA
[g] Department of Microbiology & Immunology, Galveston, TX, USA
[h] Sealy Center for Vaccine Development, Galveston, TX, USA
[i] Sealy Center for Structural Biology & Molecular Biophysics, University of Texas Medical Branch, Galveston, TX, USA
[j] Department of Pathology, Pará State University, Belém, Brazil
[k] Department of Pharmacology & Toxicology, University of Texas Medical Branch, Galveston, TX, USA

ARTICLE INFO

Article history:
Received 4 January 2017
Received in revised form 3 February 2017
Accepted 3 February 2017
Available online 6 February 2017

Keywords:
Zika virus vaccine
Flavivirus NS1
Flavivirus assembly

ABSTRACT

A purified inactivated vaccine (PIV) using the Zika virus (ZIKV) Puerto Rico strain PRVABC59 showed efficacy in monkeys, and is currently in a phase I clinical trial. High-yield manufacture of this PIV is essential for its development and vaccine access. Here we report an infectious cDNA clone-launched platform to maximize its yield. A single NS1 protein substitution (K265E) was identified to increase ZIKV replication on Vero cells (a cell line approved for vaccine production) for both Cambodian FSS13025 and Puerto Rico PRVABC59 strains. The NS1 mutation did not affect viral RNA synthesis, but significantly increased virion assembly through an increased interaction between NS1 and NS2A (a known regulator of flavivirus assembly). The NS1 mutant virus retained wild-type virulence in the A129 mouse model, but decreased its competence to infect *Aedes aegypti* mosquitoes. To further increase virus yield, we constructed an infectious cDNA clone of the clinical trial PIV strain PRVABC59 containing three viral replication-enhancing mutations (NS1 K265E, prM H83R, and NS3 S356F). The mutant cDNA clone produced >25-fold more ZIKV than the wild-type parent on Vero cells. This cDNA clone-launched manufacture platform has the advantages of higher virus yield, shortened manufacture time, and minimized chance of contamination.

1. Introduction

Zika virus (ZIKV) has recently caused explosive outbreaks in the Americas and is unexpectedly associated with congenital microcephaly and other fetal abnormalities as well as Guillain Barré syndrome (Schuler-Faccini et al., 2016). ZIKV was first isolated from a sentinel rhesus macaque in 1947 in the Zika Forest of Uganda (Dick et al., 1952). Human ZIKV infections have only sporadically been detected for decades. However, since 2007, ZIKV has rapidly spread across islands in the South Pacific and into the Americas, causing the outbreak on Yap Island in Micronesia, a subsequent outbreak in French Polynesia, and explosive, widespread epidemics in the Americas (Petersen et al., 2016). The World Health organization (http://www.who.int/emergencies/zika-virus/situation-report/6-october-2016/en/) has reported over 73 countries and territories with active ZIKV outbreaks/epidemics. Despite urgent medical needs, neither clinically approved vaccine nor antiviral is available for prevention and treatment.

ZIKV is a mosquito-borne member from the genus *flavivirus* within the family Flaviviridae. Besides ZIKV, many other flaviviruses are significant human pathogens, including the four serotypes of dengue (DENV-1 to -4), yellow fever (YFV), West Nile (WNV), Japanese encephalitis (JEV), and tick-borne encephalitis (TBEV) viruses. Flaviviruses have a positive-sense single-stranded RNA genome approximately 11,000 nucleotides in length. The genome contains a 5′ untranslated region

* Corresponding author.
** Corresponding author at: University of Texas Medical Branch, Department of Biochemistry & Molecular Biology, 5.104A Medical Research Building, Galveston, TX 77555, USA.
E-mail addresses: xuxie@utmb.edu (X. Xie), peshi@utmb.edu (P.-Y. Shi).
[1] Y.Y. and C.S. made equal contributions to this study.

http://dx.doi.org/10.1016/j.ebiom.2017.02.003

(UTR), single open-reading frame (ORF), and 3′ UTR. The ORF encodes three structural (capsid [C], precursor membrane [prM], and envelope [E]) and seven non-structural (NS1, NS2A, NS2B, NS3, NS4A, NS4B, and NS5) proteins. The structural proteins form virus particles and function in virus entry into cells. The nonstructural proteins participate in viral replication, virion assembly, and evasion of host innate immune responses (Lindenbach et al., 2013). Like other flaviviruses, ZIKV enters cells through the receptor-mediated endocytosis. After low pH-induced fusion with the endosome membrane, flaviviruses release and translate their genomic RNA in the endoplasmic reticulum (ER). Viral RNA replication occurs in the virus-induced replication complexes formed in the ER membrane. Progeny viruses form on the ER-derived membrane as immature virus particles, in which prM/E heterodimers form trimeric spikes with icosahedral symmetry. After removal of the pr from the prM by host furin protease during the transit through the Golgi network, the immature, non-infectious virions become mature infectious viruses. Finally, progeny virions are released through an exocytosis pathway (Lindenbach et al., 2013). Rapid progress has been made on ZIKV research in the past two years, including the high-resolution structures of virus (Kostyuchenko et al., 2016; Sirohi et al., 2016), reverse genetic systems (Atieh et al., 2016; Schwarz et al., 2016; Shan et al., 2016b; Tsetsarkin et al., 2016; Weger-Lucarelli et al., 2017; Xie et al., 2016), animal models (Lazear et al., 2016; Rossi et al., 2016), and vaccine development (Abbink et al., 2016; Dowd et al., 2016; Larocca et al., 2016).

Development of an effective and affordable ZIKV vaccine is a public health priority. Multiple strategies have been taken, including DNA- or viral vector-expressing subunit, chimeric, and live-attenuated vaccines (Dawes et al., 2016). Three frontrunner candidates, including two DNA vaccines expressing viral structural proteins prM and E (Dowd et al., 2016; Larocca et al., 2016) and one purified inactivated ZIKV vaccine (PIV) based on Puerto Rico strain PRVABC59 (Abbink et al., 2016), protect monkeys from ZIKV challenge. These frontrunners are currently in phase I clinical trial (https://clinicaltrials.gov). For inactivated vaccines, technologies that could increase the yield of virus production without compromising vaccine immunogenicity are essential to reduce the cost of manufacture and to increase vaccine accessibility.

In this study, we identified and characterized a mutation in ZIKV NS1 (K265E) that significantly increased the production of the Cambodian strain FSS13025 and Puerto Rico strain PRVABC59 on Vero cells, an approved cell line for vaccine production (Griffiths, 1987). The NS1 K265E mutation increased virus assembly through enhancing the NS1/NS2A interaction. Interestingly, the NS1 K265E mutation did not affect virulence in the A129 mouse model, but significantly reduced ZIKV competence for infecting *Aedes aegypti* mosquitoes. Furthermore, we engineered a recombinant ZIKV containing three replication-enhancing mutations (NS1 K265E, prM H83R, and NS3 S356F) that could generate a viral titer of $>10^8$ PFU/ml on Vero cells. Taken together, the results demonstrate that the infectious cDNA clone containing these triple mutations represents an attractive platform to reproducibly generate high yields of ZIKV, which could be readily used for manufacture of PIV for a vaccine clinical trial.

2. Materials and Methods

2.1. Cell Culture and Antibodies

BHK-21 and Vero cells were purchased from the American Type Culture Collection (ATCC, Bethesda, MD), and maintained in a high-glucose Dulbecco's modified Eagle's medium (DMEM) supplemented with 10% fetal bovine serum (FBS) (HyClone Laboratories, South Logan, UT) and 1% penicillin/streptomycin at 37 °C with 5% CO_2. *A. albopictus* C6/36 cells were grown in RPMI1640 containing 10% FBS and 1% penicillin/streptomycin at 30 °C with 5% CO_2. Huh7 cells were maintained in a high-glucose Dulbecco's Modified Eagle Medium (DMEM) supplemented with 10% fetal bovine serum (FBS), 1% penicillin/streptomycin and 1% Non-Essential Amino Acids (NEAA) at 37 °C with 5% CO_2. HEK293T cells were grown in high-glucose DMEM containing 10% FBS and 1% penicillin/streptomycin. All culture medium, NEAA and antibiotics were purchased from ThermoFisher Scientific (Waltham, MA).

The following antibodies were used: a mouse monoclonal antibody (mAb) 4G2 cross-reactive with flavivirus E protein (ATCC); goat anti-mouse IgG conjugated with Alexa Fluor®488 (Thermo Fisher Scientific, Waltham, MA); goat anti-mouse or anti-rabbit IgGs conjugated with horseradish peroxidase (IgG-HRP), protein A conjugated with HRP (A-HRP; Sigma, St. Louis, MO); rabbit or mouse control IgGs (ThermoFisher Scientific); rabbit IgG against ZIKV NS1, mouse IgG anti-ZIKV E, rabbit IgG anti-ZIKV prM (Alpha Diagnostic Intl. Inc., San Antonio, TX); mouse anti-HA (Abcam, Cambridge, United Kingdom); and rabbit anti-HA (Sigma).

2.2. Plasmid Construction

The NS1 K265E mutation was introduced into the ZIKV infectious clone pFLZIKV containing the cDNA sequence of Cambodian strain (FSS13025) (Shan et al., 2016b) through an overlap PCR approach. Briefly, a cDNA fragment flanked between restriction sites *Avr*II (positions 1532-1537 in ZIKV genome) and *Sph*I (positions 3856-3861 in ZIKV genome) was amplified by overlap PCR. The A3282G (NS1 K265E) mutation was introduced into the overlap primers during primer synthesis. The overlap PCR product containing the A3282G mutation was digested with AvrII and SphI restriction enzymes and cloned into the pFLZIKV.

Prior to construction of the infectious clone of ZIKV strain PRVABC59 (ZIKV-PRV), the parental viruses were propagated on Vero cells for two passages and subjected to whole-genome sequencing. Specifically, viral RNA was extracted using QIAamp Viral RNA Kits (Qiagen, Hilden, Germany). cDNA fragments covering the complete genome were synthesized from genomic RNA using the SuperScript® III One-Step RT-PCR System with Platinum® Taq DNA Polymerase (Invitrogen) according to the manufacturer's instructions. Similar strategy as previously reported for making ZIKV FSS13025 infectious clone (Shan et al., 2016b) was used to construct the infectious clone of ZIKV-PRV. Fig. 3A depicts the scheme to clone and assemble the full genome of ZIKV-PRV. The genomic cDNA was assembled using a single-copy vector pCC1BAC (Epicentre, Madison, WI). *E. coli* strain TransforMax™ EPI300™ (Epicentre) was used to propagate the plasmids. The virus-specific sequence of each intermediate clone was validated by Sanger DNA sequencing before it was used in subsequent steps. The final plasmid containing full-length cDNA (pFLZIKV-PRV) was sequenced to ensure no undesired mutations. A T7 promoter and a hepatitis delta virus ribozyme (HDVr) sequence were engineered at the 5′ and 3′ ends of the complete viral cDNA for *in vitro* transcription and for generation of the authentic 3′ end of the RNA transcript, respectively. All restriction endonucleases were purchased from New England Biolabs (Beverly, MA).

A mammalian expression vector, pXJ (Xie et al., 2013), driven by a cytomegalovirus (CMV) promoter was used to express the polyprotein E_{24}-NS1-NS2A-HA of ZIKV strain FSS13025. The C-terminal 24 amino acids of the E protein were retained to ensure the correct targeting and processing of NS1 in the ER membrane. The gene cassette encoding E_{24}-NS1-NS2A was amplified from pFLZIKV (Shan et al., 2016b) by PCR using primer pair P1 (5′-GATGCGGCCGCACCATGAATGGATCTATTTCCCTTATGTGCTTG-3′) and reverse primer P2 (5′-TAATCTGGAACATCGTATGGGTAGGATCCCCGCTTCCCACTCCTTGTGAGC-A-3′). The human influenza hemagglutinin (HA) tag (GSYPYDVPDYA) sequence was in-frame fused to the C-terminus of NS2A through a second PCR using primer P1 and P3 (5′-GACCTCGAGCTAAGCGTAATCTGGAACATCGTATGGGTAGGATCC-3′). The purified PCR fragment was cloned into pXJ vector through restriction enzymes *Not*I and *Xho*I. All plasmids were validated by restriction enzyme digestion and DNA sequencing from GENEWIZ (South Plainfield, NJ). Other primer sequences and the complete pFLZIKV-PRV sequence are available upon request.

2.3. RNA In Vitro Transcription, Electroporation and Immunofluorescence Assay

Plasmid linearization, RNA *in vitro* transcription and Vero cell electroporation were performed according to previously described protocols (Shan et al., 2016b). After electroporation, cells were seeded in a T-175 flask for virus production or 8-well chamber slide for monitoring E protein expression by immunofluorescence assay (IFA). IFA was performed as described previously (Shan et al., 2016b). Antibody 4G2 and goat anti-mouse IgG conjugated with Alexa Fluor®488 were used as primary and secondary antibodies, respectively. Finally, the cells were mounted in a mounting medium with DAPI (4′, 6-diamidino-2-phenylindole; Vector Laboratories, Inc., Burlingame, CA). Fluorescence images were acquired by a fluorescence microscope equipped with a video documentation system (Olympus, Shinjuku, Tokyo, Japan).

2.4. Virus Replication Kinetics and Plaque Assay

C6/36 cells (1.2×10^6 cells/well), BHK-21 cells (8×10^5 cells/well), Vero cells (8×10^5 cells/well) or Huh7 cells (8×10^5 cells/well) were seeded into a 6-well plate one day prior to infection. At 16–20 h post-seeding, cells were infected with WT or mutant ZIKV at an MOI 0.01. Infection was performed in triplicate at 30 °C (C6/36 cells) or 37 °C (BHK-21, Vero and Huh7 cells). After 1 h incubation, virus inoculum was removed and cells were washed extensively by PBS to eliminate unabsorbed viruses. Afterwards, 3 ml fresh medium was added to each well. From day 1 to 6 post-infection, supernatants were collected daily and clarified by centrifugation at 500 g for 5 min prior to storage at −80 °C. Virus in the culture fluids were determined by standard cytopathogenic effect-based plaque assay on Vero cells (Shan et al., 2016b). Plaques formed on Vero monolayers were stained by crystal violet after 4 days of infection.

2.5. Replicon Transient Transfection Assay

This assay was performed as described previously (Xie et al., 2016). WT or NS1 K265E (10 μg) ZIKV FSS13025 replicon RNAs were electroporated into Vero cells. At given time points, cells were washed twice with PBS and lysed in 100 μl 1× *Renilla* luciferase lysis buffer (Promega, Madison, WI). Luciferase signals were immediately measured by Cytation 5 (Biotek, Winooski, VT) according to the manufacturer's instructions.

2.6. Plaque Purification

Vero cells (8×10^5 per well) were seeded into a 6-well plate. At 18–24 h post-seeding, 200 μl serial dilutions of ZIKV (10^2 to 10^5 PFU/ml) were inoculated onto the monolayer for infection at 37 °C for 1 h. Afterwards, virus inoculants were replaced with 3 ml of the first overlay (DMEM supplemented with 3.7 g/L $NaHCO_3$, 2% FBS [v/v], 1% penicillin/streptomycin [v/v] and 1% Lonza SeaPlaque™ agarose [w/v]). Plates were incubated at 37 °C with 5% CO_2. After four days of incubation, 3 ml of the second overlay (first overlay supplemented with 1/50 0.33% neutral red solution [Sigma]) was added to the top of the first layer. Plates were incubated at 37 °C with 5% CO_2 for another two days. Sequentially, individual plaques were harvested and transferred into a 24-well plate pre-seeded with 2×10^5 Vero cells. After 2–3 days of incubation, cytopathic effects occurred in 24-well plates. Immediately, supernatants were harvested, clarified by centrifugation at 500 g for 5 min and stored at −80 °C. The titers and plaque morphologies of all isolates were determined by plaque assay (Shan et al., 2016b). The cDNA sequence of the viral genomes from three large and three small plaque isolates were determined by Sanger sequencing.

2.7. Quantitative Reverse Transcription PCR (qRT-PCR)

Viral RNAs in culture fluids were extracted using QIAamp viral RNA minikit (Qiagen), and intracellular total RNAs were isolated using an RNeasy minikit (Qiagen). Extracted RNAs were eluted in 50 μl RNase-free water. One specific probe (5′-FAM/AGCCTACCT/ZEN/TGACAAGCAATCAGACACTCAA/3IABkFQ-3′) and a primer set (ZIKV_1193F: 5′-CCGCTGCCCAACACAAG-3′; ZIKV_1269R: 5′-CCACTAACGTTCTTTTGCAGACAT-3′) were used to determine the ZIKV RNA copies. The probe contains a 5′-FAM reporter dye, 3′ IBFQ quencher, and internal ZEN quencher. qRT-PCR assays were performed on the LightCycler® 480 System (Roche) following the manufacturer's protocol by using 15-μl reactions of the QuantiTect Probe RT-PCR Kit (QIAGEN) and 1.5 μl RNA templates. *In vitro* transcribed full-length ZIKV RNAs were used as RNA standard for RT-PCR quantification. The mRNA level of the housekeeping gene glyceraldehyde-3-phophate dehydrogenase (GAPDH) was measured using an iScript one-Step RT-PCR kit with SYBR green (Bio-Rad) and a primer pair M_GAPDH-F (5′-AGGTCGGTGTGAACGGATTTG-3′) and M_GAPDH-R (5′-TGTAGACCATGTAGTTGAGGTCA-3′).

2.8. Quantification of Extra- and Intracellular Infectious Virions

At selected time points, about 1 ml of culture fluids were harvested and centrifuged at 500*g* for 5 min to remove cell debris prior to storage at −80 °C. Infected cells were washed three times with cold PBS to remove unbound virions. As indicated in Fig. 4, a stringent wash in cold alkaline-high-salt solution (1 M NaCl and 50 mM sodium bicarbonate, pH 9.5) for 3 min was applied to remove cell surface-associated virus. After twice cold-PBS washes, the cells were detached using 0.25% Trypsin-EDTA (ThermoFisher Scientific) and suspended in 3 ml DMEM medium containing 2% FBS. Total cells were collected by centrifugation at 1000*g* for 5 min. The cell pellets were resuspended in 250 μl DMEM medium with 2% FBS. One hundred microliters of the cell suspensions was centrifuged at 1000*g* for 5 min to pellet the cells; the pelleted cells were then used for intracellular viral RNA. The remaining 150 μl of cell suspensions was lysed using a single freeze-thaw cycle (frozen at −80 °C and thawed at 37 °C). Afterwards, cellular debris was removed by centrifugation at 3200*g* for 5 min at 4 °C, and the supernatant was harvested for plaque assay to determine the intracellular infectivity.

2.9. Co-Immunoprecipitation (Co-IP)

Co-IPs were performed according to a previous described protocol (Zou et al., 2014) with some modifications. For infection samples, 3×10^6 Vero cells in 6-cm dishes were infected with recombinant WT or NS1 K265E ZIKV strain FSS13025 at MOI 1.0. At 32 h p.t., cells were washed three times with PBS and lysed in 1 ml Pierce™ IP lysis buffer at 4 °C for 30 min. For transfection samples, 3×10^6 HEK293T cells in 6-cm dishes were transfected with 5 μg of plasmids encoding WT or NS1 K265E mutated polyprotein E_{24}-NS1-NS2A-HA using X-tremeGENE 9 DNA transfection reagent (Roche) according to the manufacturer's instructions. At 42 h p.t., cells were washed twice with cold PBS an lysed in 1 ml immunoprecipitation (IP) buffer (20 mM Tris, pH 7.5, 100 mM NaCl, 0.5% DDM, and EDTA-free protease inhibitor cocktail [Roche]) with rotation at 4 °C for 1 h. All cell lysates were clarified by centrifugation at 15000 rpm at 4 °C for 30 min and subjected to co-IP using protein G-conjugated magnetic beads according to the manufacturer's instructions (Millipore). Briefly, immune complexes were formed at 4 °C overnight by mixing 400 μl of cell lysate with 2 μg corresponding antibodies (rabbit anti-NS1, mouse anti-HA, rabbit control IgGs or mouse control IgGs) in a 500-μl reaction system containing 300 mM sodium chloride. Subsequently, the complexes were precipitated with protein G-conjugated magnetic beads at 4 °C for 1 h with rotation, followed by washing extensively with phosphate-buffered saline (PBS) containing 0.1% Tween 20 (Sigma). Finally, proteins were eluted with 4× lithium

dodecyl sulfate (LDS) sample buffer (ThermoFisher Scientific) supplemented with 100 mM DTT, heated at 70 °C for 10 min, and analyzed by Western blotting described as below.

2.10. SDS-PAGE and Western Blotting

Proteins were resolved in 12% SDS-PAGE gels and transferred onto a polyvinylidene difluoride (PVDF) membrane by using a Trans-Blot Turbo transfer system (Bio-Rad Laboratories, Hercules, CA). The blots were blocked in TBST buffer (10 mM Tris-HCl, pH 7.5, 150 mM NaCl, and 0.1% Tween 20) supplemented with 5% skim milk for 1 h, followed by probing with primary antibodies (1:2000 dilution) for 1 h at room temperature. After two washes with TBST buffer, the blots were incubated with a goat anti-mouse or goat anti-rabbit IgG conjugated to HRP (1:20,000 dilution) in TBST buffer with 5% milk for 1 h, followed by three washes with TBST buffer. The antibody-protein complexes were detected using Amersham ECL Prime Western blotting detection reagent (GE Healthcare, Chicago, IL).

2.11. Mouse Experiments

A129 mice (interferon type I receptor-knockout) were used to examine the virulence of recombinant WT or NS1 K265E ZIKV FSS13025. Experiments were performed according to a previously described protocol with some modifications (Shan et al., 2016b). In brief, 6-week-old A129 mice were infected with 10^4 PFU via the intraperitoneal route. Eight mice were used for each group. Calcium and magnesium-free DPBS (ThermoFisher Scientific) was used to dilute the virus stocks to the desired concentration. DPBS injection was used as mock-infection. On day 1–4 post-infection, four mice from each cohort were bled via the retro-orbital sinus (RO) after being anesthetized. Serum was clarified by centrifugation at 6000*g* for 5 min and immediately stored at −80 °C prior to plaque assay for viremia. All animal work was completed in compliance with the UTMB policy as approved by the Institutional Animal Care and Use Committee (IACUC).

2.12. Infection of Mosquitoes with ZIKV

Aedes aegypti colony mosquitoes derived from Galveston, TX, were fed for 30 min on blood meals. The blood meals consist of 1% (wt/vol) sucrose, 20% (vol/vol) FBS, 5 mM ATP, 33% (vol/vol) PBS-washed human blood cells (UTMB Blood Bank), and 33% (vol/vol) DMEM medium. The 1 ml-blood meals were combined with 1 ml virus offered in Hemotek 2-ml heated reservoirs (Discovery Workshops) covered with a mouse skin. Virus titer in the blood meals ranged from 6.0 to 6.5 $\log_{10}$ PFU/ml. Infectious blood meals were loaded on cartons containing *A. aegypti*. Engorged mosquitoes were incubated at 28 °C, 80% relative humidity on a 12:12 h light:dark cycle with ad libitum access to 10% sucrose for 14 days, then frozen at −20 °C overnight. To assess infection, whole bodies of individual mosquitoes were individually homogenized (Retsch MM300 homogenizer, Retsch Inc., Newton, PA) in DMEM with 20% FBS and 250 μg/ml amphotericin B. The samples were then centrifuged for 10 min at 5000 rpm. Afterwards, 50 μl of supernatants were inoculated into 96-well plates containing Vero cells at 37 °C and 5% CO_2 for 3 days. Cells were fixed with a mixture of ice-cold acetone and methanol (1:1) solution and immunostained as described previously (Shan et al., 2016b). The infection rate was calculated using the number of virus-positive mosquito bodies divided by the total number of engorged and incubated mosquitoes.

3. Results

3.1. Identification of NS1 K265E Mutation

To identify cell-adaptive mutation(s) that can increase the yields of ZIKV production on Vero cells, we used a one-step plaque-purification approach to isolate virus clones with increased replication competency using Cambodian strain FSS13025. This ZIKV strain was isolated in 2010 from the blood of a three-year old patient from Cambodia (Heang et al., 2012), and had been cultured thrice on Vero cells. This parental isolate generated heterogeneous plaque sizes on Vero cells (Fig. 1A, left panel), from which we purified viruses three large (S1–3) and three small plaques (S4–6). Representative plaque morphologies of the purified viruses are shown in Fig. 1A (right panels). Complete-genome sequencing was performed for the purified S1–6 viruses (Fig. 1B). All three large plaque biological clones (S1–3) shared an adenine-to-guanine substitution at genomic position 3282 (A3282G; GenBank KU955593.1), resulting in a Lys-to-Glu change at the position 265 in NS1 protein (K265E). The sequence chromatograph showed a highly homogeneous A3282G mutation for S1–3 viruses, whereas no such mutation was recovered in any of the S4-6 biologically cloned viruses exhibiting small plaques (Fig. 1C). The results suggested that NS1 K265E mutation may enhance ZIKV replication on Vero cells.

3.2. Characterization of Recombinant NS1 K265E ZIKV FSS13025

Since mutations other than NS1 K265E were also recovered from S1-3 viruses, we engineered the NS1 K265E mutation into the ZIKV strain FSS13025 to verify its role in increased plaque morphology. Both WT and NS1 K265E mutant genomic RNAs were electroporated into Vero cells. An increasing number of the transfected cells expressed viral E protein from 24 to 72 h post-transfection (p.t.); interestingly, the K265E mutant RNA produced more E-positive cells than the WT at 48 and 72 h p.t. (Fig. 1D). In addition, this mutant produced larger plaques than the WT virus (Fig. 1E).

To examine the effect of NS1 K265E on viral infectivity, we determined the RNA copy/plaque-forming unit (PFU) ratio for both WT and NS1 K265E viruses. The extracellular viral RNA copies represented total virus (including both infectious and non-infectious) released into the culture fluids, while the PFU numbers indicated the amounts of infectious virions. Both the WT and mutant (collected at 72 h p.t.) showed similar RNA copy/PFU ratios (Fig.1F), indicating that NS1 K265E did not affect viral infectivity. Corroborating the plaque assay and IFA results, the mutant RNA yielded significantly more infectious virus than the WT RNA after transfection of cells (Fig. 1G). Genomic sequencing of the recombinant mutant virus revealed no mutations other than the engineered NS1 K265E change (data not shown). Collectively, the results demonstrated that the NS1 K265E mutation was responsible for the enhanced ZIKV replication on Vero cells.

3.3. Comparison of Viral Replication of WT or NS1 Mutant ZIKV FSS13025 in Cell Culture

We compared the replication kinetics of WT and NS1 K265E viruses in mosquito (C6/36), hamster (BHK-21), monkey (Vero), and human (Huh7) cell lines. Interestingly, the mutant and WT viruses showed comparable replication kinetics on C6/36 and BHK-21 cells (Fig. 2A–B). In contrast, the mutant virus replicated much faster than the WT virus on Vero and Huh7 cells (Fig. 2C–D). Specifically, the mutant virus peaked at 84 h p.i. with a titer up to 10^7 PFU/ml on Vero cells. Overall, the data suggested that NS1 K265E improved viral replication in a cell type-dependent manner.

3.4. NS1 K265E Mutation Enhances the Replication of ZIKV Strain PRVABC59 in Vero Cells

To examine whether the effects of NS1 K265E on viral replication is ZIKV strain-dependent, we engineered this mutation into a new infectious cDNA clone of ZIKV Puerto Rico strain PRVABC59 (GenBank number KU501215) isolated in 2015 (Lanciotti et al., 2016). We chose PRVABC59 because this strain was previously used to produce an inactivated vaccine [with monkey efficacy (Abbink et al., 2016)] that is

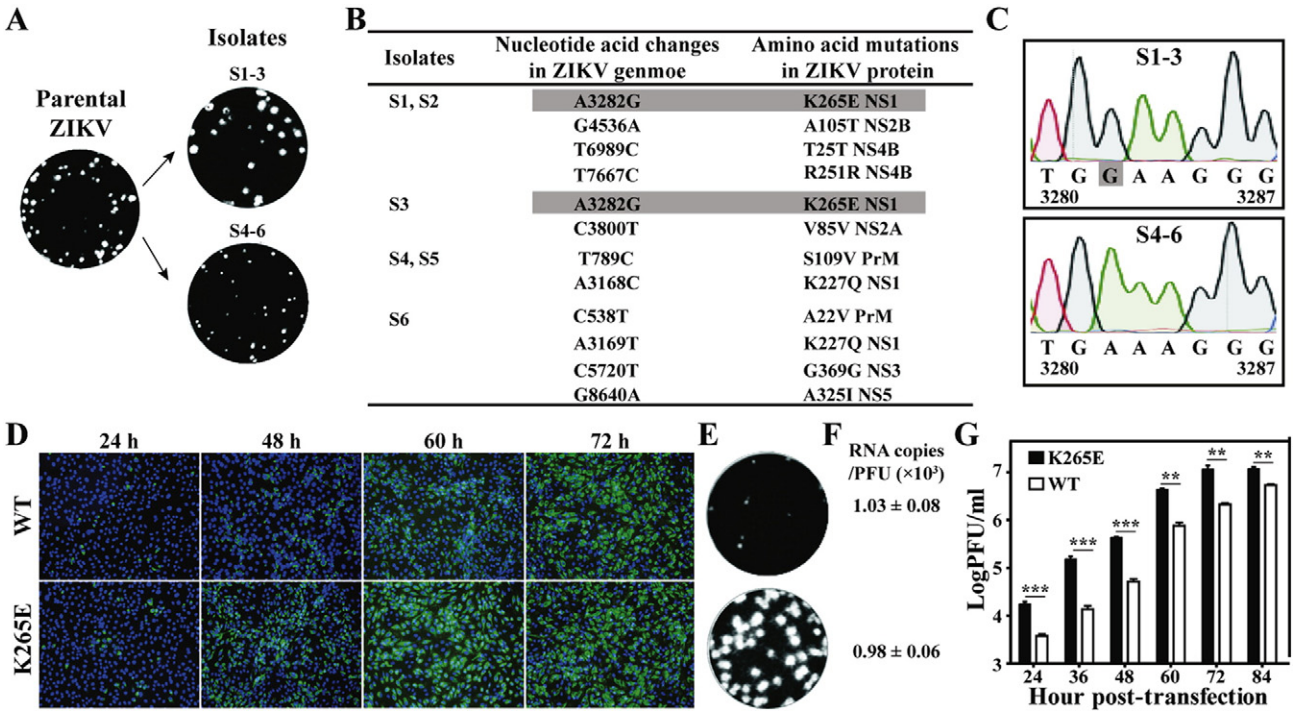

Fig. 1. Identification and characterization of NS1 K265E mutant ZIKV strain FSS13025. (A) Plaque morphologies after plaque purification. Plaques were developed on day 4 post-infection. (B) Sequence comparison of the isolates S1–6 with parental ZIKV strain FSS13025 (GenBank number KU955593.1). The nucleotide acid and amino acid changes in associated ZIKV proteins are shown. The NS1 K265E mutation is shadowed in gray. (C) cDNA sequence chromatogram of positions 3280–3287 in ZIKV. The A3283G mutation is highlighted. (D) Examination of E protein expression by immunofluorescence analysis (IFA). Vero cells were electroporated with *in vitro*-transcribed genome-length ZIKV FSS13025 (WT or K265E mutant) RNA. Intracellular E protein expression was monitored by IFA using 4G2 antibody. (E) Plaque morphologies of recombinant WT or NS1 K265E ZIKV strain FSS13025. Plaques were developed on day 4 post-infection. (F) RNA copy/PFU ratios at 72 h post-transfection. (G) Virus yields post-transfection. The extracellular virions were determined by plaque assay. Each data represents the average and standard deviation from triplicates. The multiple *t*-test was applied to examine the statistical significance between K265E and WT at indicated time points. $^{*}p < 0.05$, significant; $^{*}p < 0.01$, very significant; $^{***}p < 0.001$, extremely significant.

currently in phase I clinical trials (https://clinicaltrials.gov). As depicted in Fig. 3A, six RT-PCR fragments spanning the complete viral genome were individually cloned and assembled into the full-length cDNA of ZIKV in a single-copy vector pCC1BAC, resulting in plasmid pFLZIKV-PRV. The plasmid could be induced to generate 10–20 copies/cell using L-arabinose in *E. coli* strain TransforMax™ EPI300™. Compared with the parental ZIKV isolate, the infectious cDNA clone had five nucleotide mutations (A1337G, A2768T, A2771G, T8408A and C9176T), none of which changed the amino acid sequence (Fig. 3B).

The RNA transcribed from pFLZIKV-PRV was infectious, as evidenced by increasing E-positive cells upon transfection into Vero cells (Fig. 3C). The culture fluids harvested from WT ZIKV-PRV RNA-transfected cells produced plaques on Vero cells on day 4 p.i. (Fig. 3D). More importantly, the NS1 K265E mutant RNA-transfected cells showed a faster increase in E-positive cell numbers (Fig. 3C) than the WT. The NS1 K265E virus produced larger plaques than the WT ZIKV-PRV (Fig. 3D). The mutant RNA and virus replicated significantly faster than the WT counterparts in transfected (Fig. 3E) and infected Vero cells (Fig. 3F), respectively. These data demonstrated that the replication enhancement of NS1 K265E was not ZIKV strain-dependent.

3.5. NS1 K265E Mutation Enhances Virus Assembly, but Retards Virus Entry

To understand which step(s) of the viral infection cycle were affected by NS1 K265E mutation, we engineered the mutation into a luciferase reporter ZIKV replicon (Xie et al., 2016). After transfection of Vero cells with equal amounts of replicon RNAs, the WT and mutant produced comparable amounts of luciferase activity 2–46 h p.t. (Fig. 4A). The replicon results demonstrated that NS1 K265E mutation did not affect viral translation or RNA synthesis.

Next, we used recombinant Cambodian FSS13025 virus to examine the effect of the NS1 K265E mutation on a single infection cycle. Fig. 4B depicts the experimental flowchart. The total infection time was restricted to 20 h to avoid multiple rounds of infection. Vero cells were infected with equal amounts of WT and NS1 K265E mutant viruses at 37 °C. After 1 h p.i., cells were washed with PBS to remove unattached viruses. Intracellular viral RNAs were quantified at 1, 14, and 20 h post-infection. Before extracting intracellular viral RNA, the cells were thoroughly washed with an alkaline high-salt solution to remove cell membrane-associated viruses. Besides intracellular viral RNA, we also measured intracellular and extracellular virions (using plaque assay) as well as extracellular viral RNAs at 14 and 20 h p.i. (Fig. 4C). Compared with the WT, the K265E mutant produced slightly more intracellular viral RNA, but generated >10-fold more extracellular viral RNA as well as >10-fold more intracellular and extracellular infectious viruses at 14 and 20 h p.i. (Fig. 4C). The data indicated that NS1 K265E mutation increased virus assembly in Vero cells.

Surprisingly, at 1 h p.i., the intracellular level of mutant viral RNA of was about half of the WT virus (Fig. 4C), suggesting that the mutation reduced virus attachment/entry. This observation prompted us to perform the experiment outlined in Fig. 4D to dissect the effect of NS1 K265E on virus attachment and/or entry. Vero cells were incubated with equal amounts of WT or mutant virus at 4 °C for 1 h. At this temperature, viruses could attach to the cell surface without entry. Both WT and mutant viruses bound to Vero cells with equal efficiencies (Fig. 4E, data set I). Further incubation at 37 °C initialized virus entry. After 0.5 h incubation at 37 °C, the amount of intracellular mutant RNA was about 60% of the intracellular WT RNA (Fig. 4E, data set II); however, after additional 2.5 and 5.5 h incubation at 37 °C, equal amounts of intracellular viral RNAs were detected for mutant and WT viruses (Fig. 4E, data set III&IV). Taken together, the results suggested that, besides enhancement of virion assembly, NS1 K265E may slow virus entry (Fig. 4F).

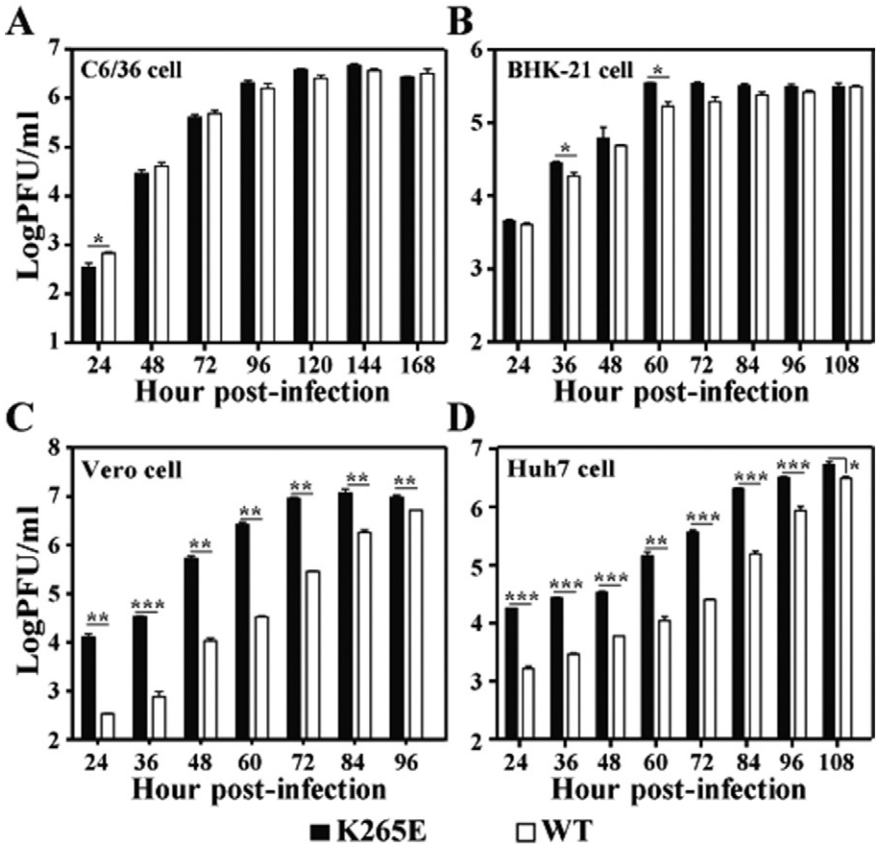

Fig. 2. Comparison of growth kinetics of NS1 K265E mutant and WT ZIKV stain FSS13025 on four different cell lines. (A) C6/36 cells. (B) BHK-21 cells. (C) Vero cells. (D) Huh7 cells. Each data represents the average and standard deviation from two independent experiments performed in triplicates. The multiple *t*-test was performed to analyze the statistical significance at each time point. Only significant differences are shown.

3.6. Mutation K265E Increases NS1/NS2A Interaction

The structure of ZIKV NS1 consists of an N-terminal β-roll, an epitope-rich wing domain, and a C-terminal β-ladder (Brown et al., 2016). Residue K265 is located at the C-terminal β-ladder, and is spatially clustered with two other positively charged residues (R294 and R347) on the surface of the NS1 molecule (Fig. 5A), suggesting that this region may participate in protein/protein interactions. Since NS1 was reported to interact with structural protein prM and E during virus assembly (Scaturro et al., 2015), we performed co-immunoprecipitation to examine whether mutation K265E affected those interactions (Fig. 5B). Western blotting of total cell lysates (collected at 32 h p.i.) showed higher levels of NS1, prM, and E protein expression in the mutant virus-infected cells than those in the WT-infected cells (Fig. 5C, right two lanes). This was expected because the mutant virus replicated more robustly than the WT. Interestingly, both prM and E proteins were co-immunoprecipitated by NS1 in the WT- and mutant-infected cells (Fig. 5C). Quantification (by normalizing the NS1 protein amounts) showed that WT and mutant K265E NS1 pulled down the prM or E protein at comparable efficiencies (Fig. 5D), indicating that the mutation did not affect the NS1/prM or NS1/E interactions.

Since NS2A is known to modulate flavivirus assembly (Kummerer and Rice, 2002; Leung et al., 2008; Xie et al., 2013), we tested whether K265E changed the NS1/NS2A interaction. Due to the lack of availability of specific antibodies against ZIKV NS2A, we performed the co-immunoprecipitation experiment using a plasmid co-expressing NS1 and HA-tagged NS2A proteins. As shown in Fig. 5E, a plasmid encoding the polyprotein E_{24}-NS1-NS2A-HA (E_{24} representing the last 24 amino acids of E protein to keep the correct topology of NS1-NS2A-HA on the ER membrane) was transfected into HEK293T cells. Upon translation, the polyproteins would be processed into E_{24}, NS1, and NS2A-HA by host signalases (Lindenbach et al., 2013). Cell lysates were immunoprecipitated by mouse anti-HA IgG or control IgG. NS1 could be pulled down together with NS2A-HA by the mouse anti-HA IgG, but not by the control IgG (Fig. 5F), demonstrating that NS1 interacted specifically with NS2A. Importantly, NS2A-HA pulled down significantly (1.2-fold) more K265E NS1 than the WT NS1 (Fig. 5G), suggesting that the mutation increased the binding of NS1 to NS2A. It should be noted that two species of NS2A-HA protein appeared in the denature SDS-PAGE (Fig. 5F), probably due to unknown modification(s) or degradation of NS2A-HA. The nature of the two NS2A-HA species remains to be determined.

3.7. NS1 K265E Mutation Does Not Affect ZIKV Virulence in the A129 Mouse Model

We evaluated the in vivo virulence of WT and mutant NS1 K265E ZIKVs in the A129 mice by monitoring the viremia and weight loss (Shan et al., 2016b). Equal amounts (1×10^4 PFU) of each virus were inoculated into mice via the intraperitoneal (i.p.) route. Unexpectedly, the WT and mutant viruses produced statistically indistinguishable levels of viremia (Fig. 6A) and weight loss (Fig. 6B). These data indicated that K265E did not affect ZIKV virulence in the A129 mouse model.

3.8. NS1 K265E Mutation Decreases Viral Infection of Ae. aegypti Mosquitoes

To understand whether the NS1 K265E mutation affects viral fitness in mosquitoes, we determined the oral susceptibility of *Ae. aegypti* using artificial human bloodmeals containing approximately 10^6 PFU/ml of the K265E mutant or WT virus (Shan et al., 2016b). On day 14 post-feeding, engorged mosquitos were analyzed for the presence of virus in the

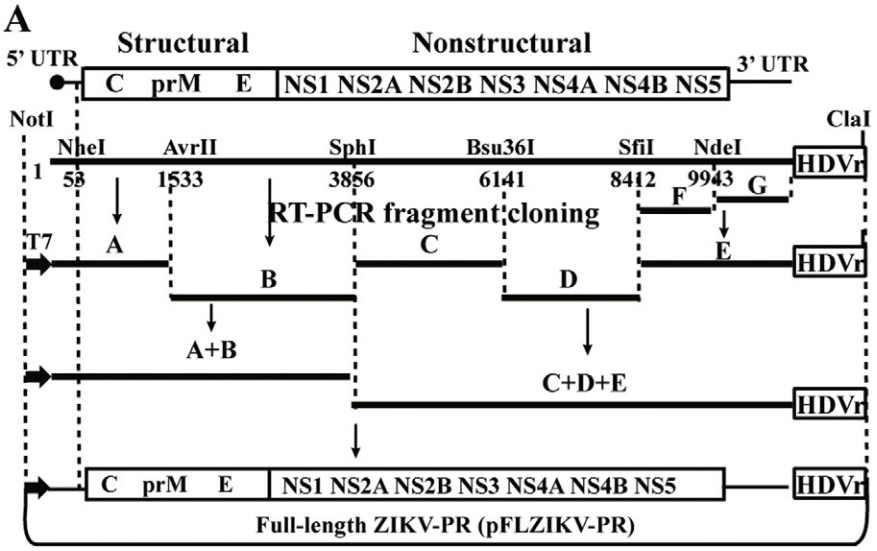

B

Nucleotide position	Parental strain	cDNA clone	Amino acid change	Location
1337	A	G	None	E
2768	A	T	None	NS1
2771	A	G	None	NS1
8408	T	A	None	NS5
9176	C	T	None	NS5

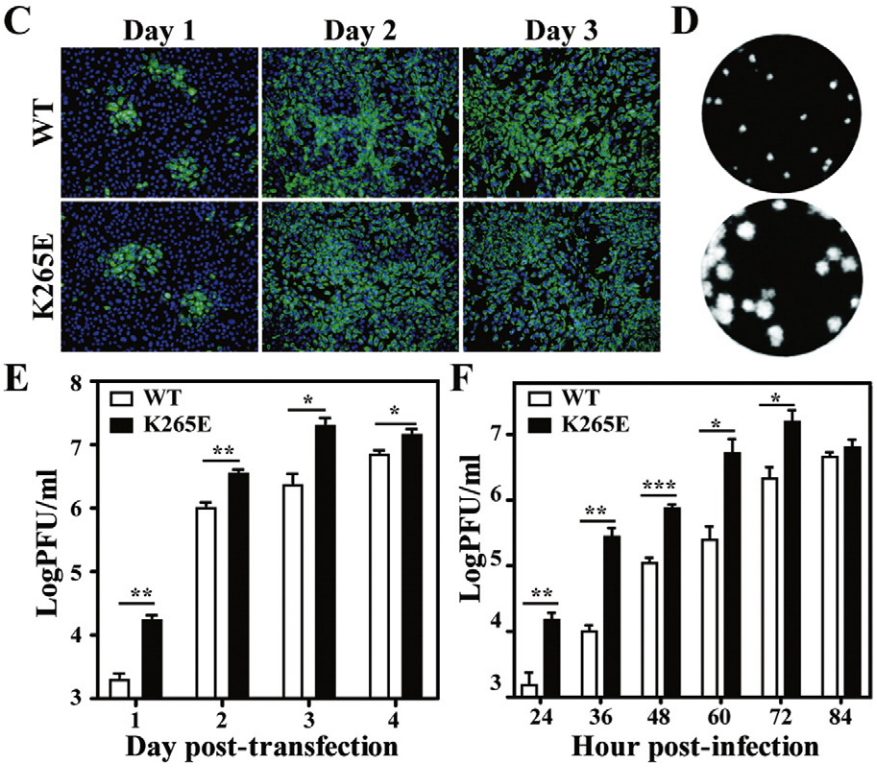

Fig. 3. Characterization of NS1 K265E in ZIKV strain PRVABC59. (A) Construction of the infectious clone of ZIKV strain PRVABC59. Six RT-PCR products (indicated as fragments A–G) were assembled to cover the complete cDNA of ZIKV genome. A T7 promoter and a hepatitis delta virus ribozyme (HDVr) sequence were engineered at the 5′ and 3′ end of the viral cDNA, respectively. Restriction enzyme sites and their nucleotide positions in ZIKV genome are indicated. (B) Sequence comparison of recombinant and parental ZIKV strain PRVABC59. (C) IFA of Vero cells transfected with *in vitro* transcribed WT or NS1 K265E mutant genome-length RNAs of ZIKV strain PRVABC59. (D) Plaque morphologies of recombinant WT or NS1 K265E ZIKV-PRV. Plaques were developed after 4 days of infection. (E) Virus yields from WT or NS1 K265E ZIKV-PRV RNA-transfected cells post-transfection. Virus titers were determined by plaque assay. (F) Growth kinetics of WT and NS1 K265E ZIKV-PRV on Vero cells. Cells were infected with WT and NS1 K265E mutant ZIKV-PRV (MOI 0.01). The multiple *t*-test was performed to analyze the statistical significance at each time point.

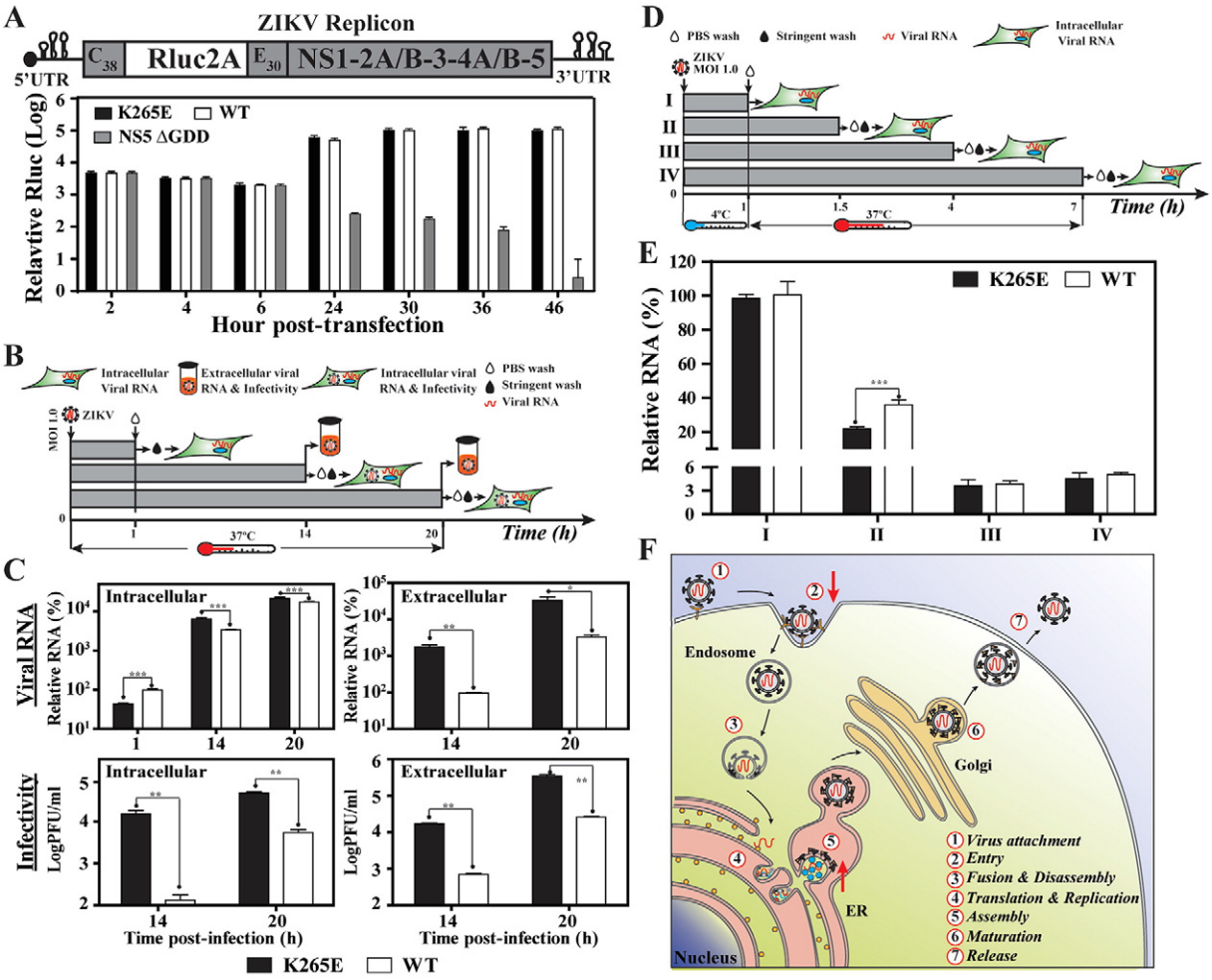

Fig. 4. Effects of NS1 K265E mutation on ZIKV life cycle. (A) Replicon transient transfection assay. The top panel shows the schematic diagram of ZIKV replicon with *Renilla* luciferase reporter. Luciferase signals of transfected cells were normalized to those of non-transfected cells. Each data point represents the average and standard deviation from three independent experiments. (B) Flowchart of monitoring single cycle of ZIKV infection. After 1-hour infection, virus inoculums were removed and cells were washed three times with PBS. To quantify intracellular viral RNAs at 1, 14 and 20 h post-infection, cells were further stringently washed. Intracellular viral RNAs were measured by qRT-PCR and normalized using the cellular GAPDH RNA levels. Extracellular viral RNA was determined by qRT-PCR; and extracellular/intracellular infectivity was quantified by plaque assay. (C) Intracellular/extracellular RNA and infectivity obtained from (B). Each data point represents the average and standard deviations of three independent experiments. The multiple *t*-test was applied to analyze the statistical significances. (D) Flowchart of examining virus attachment and entry. At given time points, intracellular viral RNAs and GAPDH RNAs were quantified by qRT-PCR accordingly. (E) Intracellular viral RNAs quantified from (D). The relative viral RNA levels were calculated by normalizing the viral RNAs at each time point to that of 1 h post-infection (set at 100%). Each data point represents the averaged relative RNA of three independent experiments. The multiple *t*-test was applied to analyze the statistical significances. (F) Carton of K265E mutation's effect on virus life cycle.

bodies to estimate infection rates. As summarized in Table 1, NS1 K265E virus showed a significantly lower infection rate than the WT virus in mosquitoes, demonstrating that the mutation reduced virus fitness for infection of *Ae. aegypti* mosquitoes.

3.9. PrM H83R and NS3 S356F Mutations Further Increase Viral Yield on Vero Cells

Although the above results demonstrated that NS1 K265E enhanced viral yield, we asked whether other cell adaptive mutations could further increase virus production on Vero cells. To address this question, we engineered two additional cell-adaptive mutations (prM H83R and NS3 S356F) in the context of NS1 K265E pFLZIKV-PRV. PrM H83R mutation was identified from passaging of ZIKV FSS13025 on Vero cells (our unpublished data). NS3 S356F mutation was recently reported to increase ZIKV replication in cell culture (Tsetsarkin et al., 2016). *In vitro* transcribed genomic RNAs (prM H83R + NS1 K265E; NS1 K265E + NS3 S356F, and prM H83R + NS1 K265E + NS3 S356F) were electroporated into Vero cells. At 72 h p.t., about 4-, 3-, and 6-fold more viruses were produced from the prM H83R + NS1 K265E, NS1 K265E + NS3 S356F, and prM H83R + NS1 K265E + NS3 S356F RNA-transfected cells than the NS1 K265E RNA-transfected cells,

Fig. 5. Co-immunoprecipitation assay (Co-IP). (A) Location of residue K265 in the 3D crystal structure of ZIKV NS1. (B) Flowchart of Co-IP experiments from ZIKV infected cells. Rabbit IgG anti-NS1 or control IgGs were used for pull down ZIKV NS1 and its associated complexes. (C) Co-IP results from (B). NS1 in both eluates and cell lysates were probed using rabbit anti-NS1 and protein A-HRP. E proteins were detected by mouse IgG anti-ZIKV and goat anti-mouse IgG-HRP. prM was examined by rabbit IgG anti-ZIKV prM and goat anti-rabbit IgG-HRP. (D) Densitometry analysis of Western blot results from (C). The band intensities of prM and E proteins in (C) were quantified and normalized to those of NS1 proteins from corresponding eluates. The efficiencies of prM and E pulled-down by WT NS1 were set as 100%. The averaged relative intensities from three independent experiments were shown. An unpaired Student *t*-test was used to estimate the statistical significance. (E) Flowchart of Co-IP from HEK293T cells transiently expressing NS1 and NS2A-HA. Cell lysates was subjected to Co-IP using mouse IgG anti-HA or mouse control IgG. (F) Western blot results from (E). NS2A-HA in the eluates and cell lysates were examined by rabbit IgG anti-HA and goat anti-rabbit IgG-HRP respectively. NS1 proteins were detected by rabbit anti-ZIKV NS1 and goat anti-rabbit IgG-HRP. (G) Densitometry analysis of Western blot results from (F). The band intensities of NS1 proteins in (F) were quantified and normalized to those of NS2A-HA proteins from corresponding eluates. An unpaired Student *t*-test was used to evaluate the statistical significance.

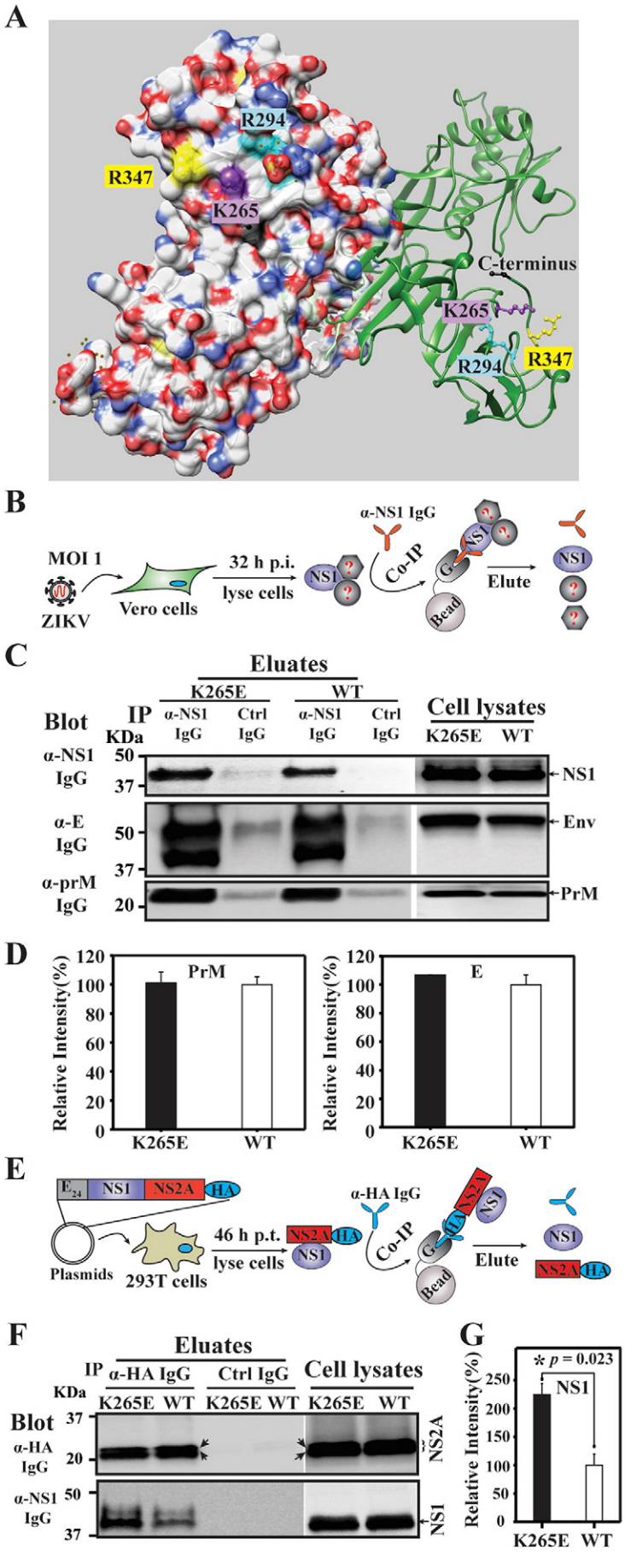
A
R294
R347
K265
C-terminus
K265
R294
R347
B
MOI 1
ZIKV
Vero cells
32 h p.i.
lyse cells
α-NS1 IgG
Co-IP
Bead
Elute
NS1
C
Eluates
K265E
WT
Blot
IP
KDa
α-NS1 IgG
Ctrl IgG
α-NS1 IgG
Ctrl IgG
Cell lysates
K265E
WT
α-NS1 IgG
α-E IgG
α-prM IgG
50
37
50
37
20
NS1
Env
PrM
D
Relative Intensity(%)
PrM
E
K265E
WT
E
NS1
NS2A
HA
Plasmids
293T cells
46 h p.t.
lyse cells
α-HA IgG
Co-IP
Bead
Elute
F
Eluates
IP
α-HA IgG
Ctrl IgG
Cell lysates
KDa
K265E WT K265E WT K265E WT
Blot
α-HA IgG
α-NS1 IgG
37
20
50
37
NS2A
NS1
G
Relative Intensity(%)
* p = 0.023
NS1
250
200
150
100
50
0
K265E
WT

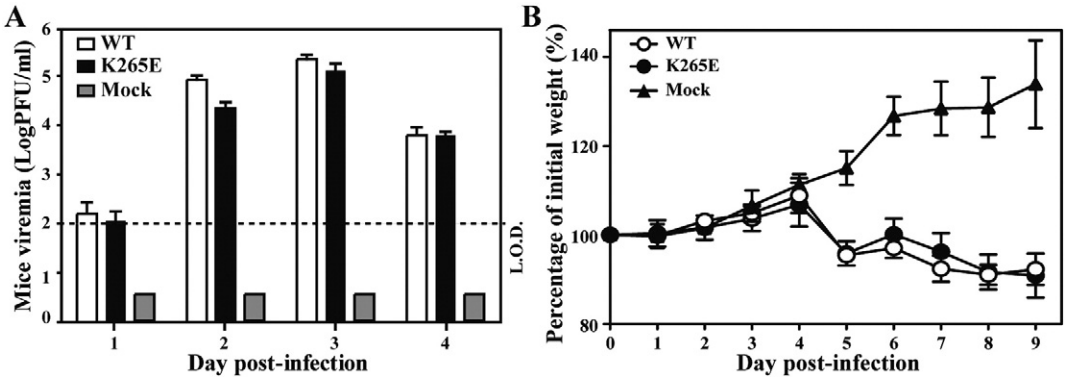

Fig. 6. Comparison of virulence between recombinant WT and NS1 K265E ZIKV strain FSS13025 in A129 mice. (A) Viremia from day 1 to 4 post-infection. Viremia was quantified using plaque assay. Limitation of detection (L.O.D.) is 100 PFU/ml. Each data point represents the averaged viremia from four mice. (B) Weight loss. The averaged percentages of initial weight from eight mice are presented. The two-way ANOVA multiple comparison was used to evaluate the statistical significance.

respectively (Fig. 7A). All three mutants generated similar plaque morphologies as the NS1 K265E virus on Vero cells (Fig. 7A). Importantly, replication kinetics showed that the triple mutant virus (prM H83R + NS1 K265E + NS3 S356F) produced a peak viral titer of 1.6×10^8 PFU/ml that was significantly higher than the other mutants (Fig. 7B). Fig. 7C directly compares the replication kinetics of the WT ZIKV PRVABC59 strain with its triple mutant. Remarkably, the triple mutant 447 generated ≥27-fold more virus than the WT at various time post-infection. The results clearly indicate that the triple mutant would be an ideal candidate for the manufacturing of inactivated vaccine.

4. Discussion

Purified inactivated vaccine (PIV) is one of the frontrunners in the rapidly evolving ZIKV vaccine pipeline. A PIV using ZIKV strain PRVABC59 completely protects rhesus macaques from ZIKV challenge (Abbink et al., 2016), and is currently undergoing a phase I clinical trial (https://clinicaltrials.gov). Licensed PIVs have been developed for TBEV and JEV (Shan et al., 2016a). Technologies that can increase the yield of virus production with shortened manufacture time will greatly reduce the cost and increase the vaccine accessibility. Here, we report a ZIKV with triple mutations (prM H83R + NS1 K265E + NS3 S356F) that greatly increased viral replication in Vero cells. Our findings will be useful for PIV manufacture because Vero cells are approved for vaccine production (Griffiths, 1987).

The NS1 K265E mutation was initially identified from plaque purification using the parental ZIKV strain FSS13025. This mutation was consistently recovered from viruses recovered from large plaques, but not from small plaques (Fig. 1A–C). Using an infectious clone of ZIKV FSS13025, we confirmed that mutation K265E in NS1 was responsible for the enhanced viral replication (Fig. 1D–G & 2C). Interestingly, the K265E mutation increased viral replication in Vero and Huh7 cells, but not in C6/36 and BHK-21 cells (Fig. 2), suggesting that the enhancement was cell type-dependent. When the same mutation was introduced into a clone derived from epidemic strain of ZIKV PRVABC59, it also increased viral replication in Vero cells (Fig. 3), indicating that its effect on viral replication was not ZIKV stain-dependent.

Mechanistically, we provided five lines of evidence that NS1 K265E modulates the steps of viral entry and assembly during an infection cycle. (i) NS1 K265E did not affect virus attachment to the cell surface (Fig. 4E), but delayed virus entry. At 1 h post-attachment at 37 °C, the mutation reduced entry by 40%; however, entry reached WT levels at 3 and 6 h post-attachment at 37 °C (Fig. 4E). (ii) The NS1 K265E had no effect on viral protein translation and RNA synthesis in a luciferase replicon assay (Fig. 4A). (iii) The NS1 K265E mutation increased virus assembly, leading to higher levels of intracellular and extracellular infectious viruses (Fig. 4C). (iv) The RNA copy/PFU ratios of WT and NS1 K265E mutant viruses were indistinguishable (Fig. 1F), suggesting that the mutation did not affect virus maturation (e.g., cellular furin-mediated cleavage of prM to pr and M proteins). (v) Both WT and NS1 K265E ZIKV FSS13025 showed similar thermostability when incubated at physiological temperatures of 37 °C or 42 °C for up to 1 h (Supplement Fig. 1), suggesting that the mutation did not affect viral thermostability.

Flavivirus entry and assembly are tightly controlled by the spatial and temporal interplays between host and viral factors. How does the NS1 K265E mutation affect both ZIKV entry and assembly? The flavivirus NS1 is a multifunctional protein involved in viral replication (Lindenbach and Rice, 1997,1999; Youn et al., 2012), virion assembly (Scaturro et al., 2015), and evasion of host immune response (Avirutnan et al., 2011; Chung et al., 2006). The crystal structure of ZIKV NS1 shows an elongated hydrophobic surface for membrane association and a polar surface that varies substantially among different flaviviruses (Brown et al., 2016). Amino acid K265, together with two nearby positively charged residues (R294 and R347), could contribute to the positive surface of the β-ladder domain of NS1 (Fig. 5A). The K265E mutation might perturb the charge in the β-ladder domain, leading to change(s) in network interactions between viral-viral or viral-host factors. Indeed, our co-immunoprecipitation experiments revealed that the mutation increased the NS1/NS2A interaction (Fig. 5F & G) without affecting the NS1/prM and NS1/E interactions. Since NS2A has been well documented to modulate flavivirus assembly (Kummerer and Rice, 2002; Leung et al., 2008; Xie et al., 2013), the increased NS1/NS2A interaction might be responsible for the enhanced virion assembly. On the other hand, because the NS1 K265E-mediated enhancement of virion production was cell type-dependent, cellular factors (e.g., proteins and/or lipids) must be involved in the process of enhanced virion assembly. Proteomic analysis of host proteins that bind to NS1 or NS2A in infected cells could be pursued to identify cellular factors important for flavivirus assembly.

The flavivirus E protein interacts with multiple cell surface receptors and attachment factors to facilitate virus entry. Many cell surface factors are reported to mediate flavivirus entry, including heat shock proteins,

Table 1
Infection of WT or NS1 K265E ZIKV FSS13025 in *Ae. aegypti*.

Virus[a]	Blood-meal titer (Log PFU/ml)[b]	Infection rate (%)*
WT	6.0	20/37 (54)
K265E	6.1	8/42 (19)

[a] After blood meal, viral titers for both parental and recombinant viruses were measured by plaque assay to ensure the accuracy of virus amounts in the blood meal.
[b] Infection rate = (number of infected mosquitos / number of engorged mosquitos) × 100%.
* $p = 0.002$, Fisher's exact test, 2-tailed.

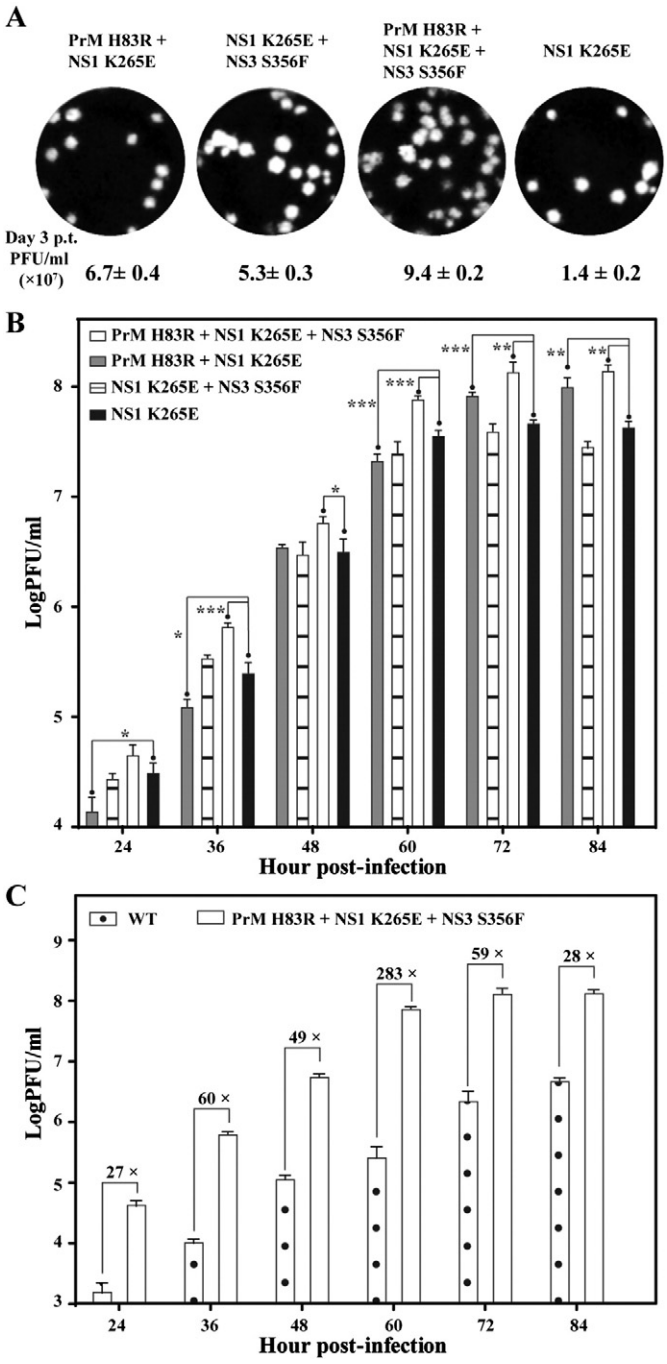

Fig. 7. PrM H83R, NS1 K265E and NS3 S356F mutations further increase viral yield. (A) Plaque morphologies. Viruses harvested on day 3 post-transfection were assayed by plaque assay on Vero cells. Plaques were developed on day 4 post-infection. (B) Growth kinetics of ZIKV-PRV mutant viruses. Vero cells were infected with equal amounts of ZIKV-PRV mutant viruses (MOI 0.01). The multiple *t*-test was performed to analyze the statistical significance at each time point. (C) Comparison of replication kinetics of the WT ZIKV PRVABC59 strain with its triple mutant. The fold differences in viral titers between the WT and triple mutant are indicated.

phosphatidylserine receptors [TIM (Tyro3, Axl, and Mer) and TAM (T cell, immunoglobulin, and mucin)], claudin-1, heparan sulfate, dendritic cell-specific intracellular adhesion molecular-3 grabbing nonintegrin (DC-SIGN), mannose receptor, and C-type lectin domain family 5 member A (Perera-Lecoin et al., 2014). ZIKV selectively binds to TAM, but not TIM phosphatidylserine transmembrane receptor (Hamel et al., 2015). The ER membrane contains phosphatidylserine lipids in the luminal leaflet (Leventis and Grinstein, 2010), and NS1 is proposed to assist in virion morphogenesis via its lipid-remodeling activity, membrane association capability, and interactions with viral non-structural and structural proteins (Scaturro et al., 2015). It is thus tempting to speculate that mutation K265E alters NS1's ability to recruit specific lipids during virion budding. The altered lipid components in virion bilayer could consequently modulate the kinetics of viral entry.

In contrast to the enhanced viral replication on Vero cells, NS1 K265E did not significantly change the virulence of ZIKV in the A129 mice (Fig. 6). The *in vitro* and in vivo discrepancy could be due to cell type-specific enhancement of the mutant virus replication (Fig. 2). In agreement with the in vivo results, NS1 K265E virus showed a WT level of viral replication on rodent BHK-21 cells (Fig. 2B). Therefore, caution should be taken when extrapolating mouse virulence result to non-human primates and humans. This is particularly important when the NS1 K265E mutation is engineered into a live-attenuated ZIKV vaccine candidate (for the purpose of increase in vaccine production on Vero cells). In such case, the effect of NS1 K265E mutation on virulence should first be directly evaluated in non-human primates.

In mosquito hosts, NS1 K265E virus replicated to the WT level on C6/36 cells, but significantly reduced its ability to infect *Ae. aegypti* (Table 1). The reduced vector infectivity of NS1 K265E ZIKV could explain its rarity in clinical isolates. Only 3 out of 169 ZIKV full-length sequences in the GenBank exhibit the NS1 K265E mutation. Since Vero cells are routinely used to isolate ZIKV, it remains to be determined whether the NS1 265E sequence from the 3 clinical isolates (GenBank number ANN83272, AOX49265, and AMS00611) resulted from adaptation to Vero cells during virus isolation.

Our study has provided a new platform to reproducibly generate high yields of ZIKV for PIV manufacture. Specifically, the infectious ZIKV cDNA clone of PRVABC59 containing the triple mutations (prM H83R + NS1 K265E + NS3 S356F) could be used to launch ZIKV production on Vero cells. The mechanism of how prM H83R and NS3 S356F mutations increase viral replication remains to be understood. In addition, further studies are needed to investigate the effect of prM H83R and NS3 S356F mutations on ZIKV virulence and vector infection. Nevertheless, compared with the traditional method of virus amplification from seed viruses, the cDNA clone-launched PIV manufacture platform has the advantages of higher yields, shortened manufacture time, higher reproducibility (viruses directly produced from *in vitro* synthesized RNA), and a reduced risk of contamination (due to the elimination of isolation and multiple rounds of passaging of seed viruses in cell culture). Since ZIKV strain PRVABC59 was used for the current PIV clinical trial, our mutant cDNA plasmid could be readily used for this vaccine manufacture.

In summary, we identified mutation NS1 K265E in ZIKV that significantly enhances the production of strains FSS13025 and PRVABC59 in Vero cell culture. Mechanistically, the NS1 K265E mutant increases virus assembly, probably through enhancing NS1/NS2A interaction. Importantly, the enhancement of virus production by the cell-adaptive triple mutations (prM H83R + NS1 K265E + NS3 S356F) and the reported reverse genetic system could be used to manufacture the ZIKV strain PRVABC59-derived PIV that is currently in phase I clinical trial.

Funding Sources

P.Y.S. was supported by University of Texas Medical Branch (UTMB) startup award, UTMB Innovation and Commercialization award, University of Texas STARs Award, NIH grant R01AI087856, Pan American Health Organization grant SCON2016-01353, and UTMB CTSA UL1TR-001439. This research was also supported by NIH grant AI120942 to S.C.W.

Conflict of Interest Statement

The authors have no conflict of interest in this study.

Author Contributions

Y.Y., C.S., J.Z., A.E.M., D.N.B., B.A.M.D., and X.X. performed the experiments. C.S., S.L.R., S.C.W., P.F.C.V., X.X., and P.Y.S. interpreted the data and wrote the manuscript.

Acknowledgements

We thank our lab members and colleagues at University of Texas Medical Branch for helpful discussions during the course of this study.

Appendix A. Supplementary Data

Supplementary data to this article can be found online at http://dx.doi.org/10.1016/j.ebiom.2017.02.003.

References

Abbink, P., Larocca, R.A., De La Barrera, R.A., Bricault, C.A., Moseley, E.T., Boyd, M., Kirilova, M., Li, Z., Ng'ang'a, D., Nanayakkara, O., et al., 2016. Protective efficacy of multiple vaccine platforms against Zika virus challenge in rhesus monkeys. Science 353, 1129–1132.

Atieh, T., Baronti, C., de Lamballerie, X., Nougairede, A., 2016. Simple reverse genetics systems for Asian and African Zika viruses. Sci. Rep. 6, 39384.

Avirutnan, P., Hauhart, R.E., Somnuke, P., Blom, A.M., Diamond, M.S., Atkinson, J.P., 2011. Binding of flavivirus nonstructural protein NS1 to C4b binding protein modulates complement activation. J. Immunol. 187, 424–433.

Brown, W.C., Akey, D.L., Konwerski, J.R., Tarrasch, J.T., Skiniotis, G., Kuhn, R.J., Smith, J.L., 2016. Extended surface for membrane association in Zika virus NS1 structure. Nat. Struct. Mol. Biol. 23, 865–867.

Chung, K.M., Liszewski, M.K., Nybakken, G., Davis, A.E., Townsend, R.R., Fremont, D.H., Atkinson, J.P., Diamond, M.S., 2006. West Nile virus nonstructural protein NS1 inhibits complement activation by binding the regulatory protein factor H. Proc. Natl. Acad. Sci. U. S. A. 103, 19111–19116.

Dawes, B.E., Smalley, C.A., Tiner, B.L., Beasley, D.W.C., Milligan, G.N., Reece, L.M., Hombach, J., Barrett, A.D.T., 2016. Research and development of Zika virus vaccines. Npj Vaccines 1, 16007.

Dick, G.W., Kitchen, S.F., Haddow, A.J., 1952. Zika virus. I. Isolations and serological specificity. Trans. R. Soc. Trop. Med. Hyg. 46, 509–520.

Dowd, K.A., Ko, S.Y., Morabito, K.M., Yang, E.S., Pelc, R.S., DeMaso, C.R., Castilho, L.R., Abbink, P., Boyd, M., Nityanandam, R., et al., 2016. Rapid development of a DNA vaccine for Zika virus. Science 354, 237–240.

Griffiths, E., 1987. Acceptability of cell substrates for production of biologicals. Report of a WHO Study Group on Biologicals. World Health Organization Technical Report vol. 747.

Hamel, R., Dejarnac, O., Wichit, S., Ekchariyawat, P., Neyret, A., Luplertlop, N., Perera-Lecoin, M., Surasombatpattana, P., Talignani, L., Thomas, F., et al., 2015. Biology of zika virus infection in human skin cells. J. Virol. 89, 8880–8896.

Heang, V., Yasuda, C.Y., Sovann, L., Haddow, A.D., Travassos da Rosa, A.P., Tesh, R.B., Kasper, M.R., 2012. Zika virus infection, Cambodia, 2010. Emerg. Infect. Dis. 18, 349–351.

Kostyuchenko, V.A., Lim, E.X., Zhang, S., Fibriansah, G., Ng, T.S., Ooi, J.S., Shi, J., Lok, S.M., 2016. Structure of the thermally stable Zika virus. Nature 533, 425–428.

Kummerer, B.M., Rice, C.M., 2002. Mutations in the yellow fever virus nonstructural protein NS2A selectively block production of infectious particles. J. Virol. 76, 4773–4784.

Lanciotti, R.S., Lambert, A.J., Holodniy, M., Saavedra, S., Signor Ldel, C., 2016. Phylogeny of zika virus in western hemisphere, 2015. Emerg. Infect. Dis. 22, 933–935.

Larocca, R.A., Abbink, P., Peron, J.P., Zanotto, P.M., Iampietro, M.J., Badamchi-Zadeh, A., Boyd, M., Ng'ang'a, D., Kirilova, M., Nityanandam, R., et al., 2016. Vaccine protection against Zika virus from Brazil. Nature 536, 474–478.

Lazear, H.M., Govero, J., Smith, A.M., Platt, D.J., Fernandez, E., Miner, J.J., Diamond, M.S., 2016. A mouse model of zika virus pathogenesis. Cell Host Microbe 19, 720–730.

Leung, J.Y., Pijlman, G.P., Kondratieva, N., Hyde, J., Mackenzie, J.M., Khromykh, A.A., 2008. Role of nonstructural protein NS2A in flavivirus assembly. J. Virol. 82, 4731–4741.

Leventis, P.A., Grinstein, S., 2010. The distribution and function of phosphatidylserine in cellular membranes. Annu. Rev. Biophys. 39, 407–427.

Lindenbach, B.D., Rice, C.M., 1997. trans-Complementation of yellow fever virus NS1 reveals a role in early RNA replication. J. Virol. 71, 9608–9617.

Lindenbach, B.D., Rice, C.M., 1999. Genetic interaction of flavivirus nonstructural proteins NS1 and NS4A as a determinant of replicase function. J. Virol. 73, 4611–4621.

Lindenbach, B.D., Murray, C.L., Thiel, H.J., Rice, C.M., 2013. Flaviviridae. In: Knipe, D.M., Howley, P.M. (Eds.), Fields Virology, sixth ed. vol. 1. Lippincott William & Wilkins, Philadelphia, pp. 712–746.

Perera-Lecoin, M., Meertens, L., Carnec, X., Amara, A., 2014. Flavivirus entry receptors: an update. Viruses 6, 69–88.

Petersen, L.R., Jamieson, D.J., Powers, A.M., Honein, M.A., 2016. Zika virus. N. Engl. J. Med. 374, 1552–1563.

Rossi, S.L., Tesh, R.B., Azar, S.R., Muruato, A.E., Hanley, K.A., Auguste, A.J., Langsjoen, R.M., Paessler, S., Vasilakis, N., Weaver, S.C., 2016. Characterization of a novel murine model to study zika virus. Am.J.Trop. Med. Hyg. 94, 1362–1369.

Scaturro, P., Cortese, M., Chatel-Chaix, L., Fischl, W., Bartenschlager, R., 2015. Dengue virus non-structural protein 1 modulates infectious particle production via interaction with the structural proteins. PLoS Pathog. 11, e1005277.

Schuler-Faccini, L., Ribeiro, E.M., Feitosa, I.M.L., Horovitz, D.D.G., Cavalcanti, D.P., Pessoa, A., Doriqui, M.J.R., Neri, J.I., Neto, J.M.D., Wanderley, H.Y.C., et al., 2016. Possible association between zika virus infection and microcephaly – Brazil, 2015. Morb. Mortal. Wkly Rep. 65, 59–62.

Schwarz, M.C., Sourisseau, M., Espino, M.M., Gray, E.S., Chambers, M.T., Tortorella, D., Evans, M.J., 2016. Rescue of the 1947 zika virus prototype strain with a cytomegalovirus promoter-driven cdna clone. mSphere 1.

Shan, C., Xie, X., Barrett, A.D., Garcia-Blanco, M.A., Tesh, R.B., Vasconcelos, P.F., Vasilakis, N., Weaver, S.C., Shi, P.Y., 2016a. Zika virus: diagnosis, therapeutics, and vaccine. ACS Infect. Dis. 2, 170–172.

Shan, C., Xie, X., Muruato, A.E., Rossi, S.L., Roundy, C.M., Azar, S.R., Yang, Y., Tesh, R.B., Bourne, N., Barrett, A.D., et al., 2016b. An infectious cDNA clone of zika virus to study viral virulence, mosquito transmission, and antiviral inhibitors. Cell Host Microbe 19, 891–900.

Sirohi, D., Chen, Z., Sun, L., Klose, T., Pierson, T.C., Rossmann, M.G., Kuhn, R.J., 2016. The 3.8 A resolution cryo-EM structure of Zika virus. Science 352, 467–470.

Tsetsarkin, K.A., Kenney, H., Chen, R., Liu, G., Manukyan, H., Whitehead, S.S., Laassri, M., Chumakov, K., Pletnev, A.G., 2016. A full-length infectious cDNA clone of zika virus from the 2015 epidemic in Brazil as a genetic platform for studies of virus-host interactions and vaccine development. MBio 7.

Weger-Lucarelli, J., Duggal, N.K., Bullard-Feibelman, K., Veselinovic, M., Romo, H., Nguyen, C., Ruckert, C., Brault, A.C., Bowen, R.A., Stenglein, M., et al., 2017. Development and characterization of recombinant virus generated from a new world zika virus infectious clone. J. Virol. 91.

Xie, X., Gayen, S., Kang, C., Yuan, Z., Shi, P.Y., 2013. Membrane topology and function of dengue virus NS2A protein. J. Virol. 87, 4609–4622.

Xie, X., Zou, J., Shan, C., Yang, Y., Kum, D.B., Dallmeier, K., Neyts, J., Shi, P.Y., 2016. Zika virus replicons for drug discovery. EBioMedicine 12, 156–160.

Youn, S., Li, T., McCune, B.T., Edeling, M.A., Fremont, D.H., Cristea, I.M., Diamond, M.S., 2012. Evidence for a genetic and physical interaction between nonstructural proteins NS1 and NS4B that modulates replication of West Nile virus. J. Virol. 86, 7360–7371.

Zou, J., Xie, X., Lee le, T., Chandrasekaran, R., Reynaud, A., Yap, L., Wang, Q.Y., Dong, H., Kang, C., Yuan, Z., et al., 2014. Dimerization of flavivirus NS4B protein. J. Virol. 88, 3379–3391.